10.1109/ULTSYM.2011.0592

Improved Synthetic Aperture Focusing Technique for Acoustic-resolution Photoacoustic Microscopy

Meng-Lin Li, Yi-Chieh Tseng and Po-Hsun Wang
Department of Electrical Engineering
National Tsing Hua University
Hsinchu, Taiwan

***Abstract*—Acoustic-resolution photoacoustic microscopy (AR-PAM) capable of imaging micro-vessels with high resolution and high contrast has shown its potential in functional neuro-vascular imaging, dermatology and related cancer research. In AR-PAM, a mechanically scanned, single crystal transducer with a fixed focus is commonly used, which causes the image quality to deteriorate significantly in the out-of-focus region. A virtual-detector based synthetic aperture focusing technique (VD-SAFT) was used previously to extend the depth of focus of the AR-PAM where the focal point of the transducer is treated as a virtual point detector. However, the performance of VD-SAFT is impaired by its high sidelobes. Such high sidelobes result from over-simplified virtual-point-detector approximation of the focal point. To solve this problem, we introduce an improved synthetic aperture focusing technique (ISAFT) for AR-PAM, which considers diffraction effect in the vicinity of the VD, i.e., the focal point. This technique is based on a linear, discrete model of the AR-PAM system developed using matrix formalism. Using this model, a spatiotemporal optimal filter in minimum mean square error sense is designed to deconvolve the spatial impulse responses associated with the focused transducer at every imaging point; thus retrospective focusing can be achieved. The performance of the proposed ISAFT is verified using simulation data. A 25-MHz AR-PAM with a single element transducer which has a 6-mm diameter and a 12-mm focal depth (i.e., f-number = 2) is simulated. The improvement in spatial resolution and sidelobe suppression of ISAFT is superior to that of VD-SAFT because the full geometry of the VD, instead of the simplified virtual-point-detector approximation, is taken into consideration. It is demonstrated by simulation that the proposed method effectively improves the degraded lateral resolution in the out-of-focused region for AR-PAM. Future work will focus on the phantom and in vivo experimental verifications and the study of the effect of signal-to-noise ratio on the ISAFT.**

Keywords-synthetic aperture focusing technique; deconvolution; spatial impulse response; photoacoustic microscopy.

I. INTRODUCTION

Photoacoustic imaging is a promising novel imaging modality which overcomes the resolution drawback of pure optical imaging due to overwhelming light scattering in biological tissues, and owns the most compelling features of both optics and ultrasound—that is, high optical absorption contrast and sub-millimeter ultrasound resolution—up to an imaging depth of centimeters[1]. It combines light and ultrasound to detect absorbed photons ultrasonically via the photoacoustic effect. In photoacoustic imaging, a short pulsed laser is employed to excite the imaging tissue for photoacoustic signal generation. Photoacoustic signals are induced due to transient thermo-elastic expansion when biological tissues are illuminated by laser pulses and then absorb the pulsed laser energy. These photoacoustic waves are then detected by ultrasonic transducers and used to form images representative of optical absorption distribution. Photoacoustic imaging has been shown as a promising tool in a wide spectrum of applications, for example, imaging of blood vessels[2][3][4], monitoring of blood oxygenation [5], and detection of melanoma and breast tumor [6], to name a few.

Recently, an *in vivo* backward-mode acoustic resolution photoacoustic microscope (AR-PAM) with dark-field illumination has been developed by Maslov et al. to image blood vessels in the skin [7]. This system is capable of imaging optical absorption contrasts with high lateral resolution (45 μm at the focal point) and high axial resolution (~15 μm) down to a 3-mm depth in biological tissue. Such AR-PAM system, i.e. high-frequency (> 20 MHz) photoacoustic imaging, offers a unique opportunity to monitor micro-vasculature[4] and thus shows potential for applications in functional neuro-vascular imaging[8], dermatology and related cancer research [6]. Here, we try to solve the imaging problems associated with the AR-PAM system. In AR-PAM, a mechanically scanned, single crystal transducer with a fixed focus is commonly used, which causes the image quality to deteriorate significantly in the out-of-focus region. A virtual-detector based synthetic aperture focusing technique (VD-SAFT) was used previously to extend the depth of focus of the AR-PAM where the focal point of the transducer is treated as a virtual point detector[9][10]. However, the performance of VD-SAFT is impaired by its high sidelobes. Such high sidelobes result from over-simplified virtual-point-detector approximation of the focal point.

To solve this problem, a model-based reconstruction method previously proposed for photoacoustic tomography with a finite-sized transducer is extended for AR-PAM[11][12] here. In this study, we introduce an improved synthetic aperture focusing technique (ISAFT) for AR-PAM, which considers diffraction effect in the vicinity of the VD,

i.e., the focal point. This technique is based on a linear, discrete model of the AR-PAM system developed using matrix formalism. Using this model, a spatiotemporal optimal filter in minimum mean square error sense is designed to deconvolve the spatial impulse responses associated with the focused transducer at every imaging point; thus retrospective focusing can be achieved. The performance of the proposed ISAFT is verified using simulation data.

II. Improved Synthetic Aperture Focusing Technique

A. Spatial impulse response

The detected signal by a finite-size transducer, from a Dirac impulse photoacoustic source and without considering the electrical impulse response of the transducer, takes the form of a finite-length pulse, depending on the position of the source and the geometry of the transducer. This finite-length pulse is called the spatial impulse response (SIR) given a detection aperture, and can be expressed as[13]

$$h_{\mathrm{SIR}}(\mathrm{r},t)=\int_{S_T}\frac{\delta(t-(|\mathrm{r}-\mathrm{r_T}|/c))}{2\pi|\mathrm{r}-\mathrm{r_T}|}dS_T, \tag{1}$$

where **r** and $\mathbf{r}_T$ are the distance vectors from the coordinate origin to the source and transducer surface, respectively, and S_T represents the transducer surface.

B. Two dimensionalimaging model of a AR-PAM system

With the SIR representation described in Eq. (1), the output signal from a photoacoustic source, detected at a given scanning position Tl of a AR-PAM system can be express as,

$$y_l(t)=h_e(t)\otimes h_{\mathrm{SIR}}(\mathrm{r},t)\otimes p(t)\cdot o(r), \tag{2}$$

where h_e(t) is the electrical impulse response of the transducer, $p(t)$ is the photoacoustic waveform, and $o(r)$ is the optical absorption determining the amplitude of $p(t)$. According to Eq. (1) and Eq. (2), a discrete linear imaging model of a AR-PAM for a scanning signle element transducer with a fixed focus is developed.

Figure 1 shows the illustration of sampling in AR-PAM data acquisition and raw data set, for matrix formalism of a two dimensional imaging model of a AR-PAM system. The transducer is linearly scanned and the measurements are taken from L positions. The ROI, **O**, is divided into M x N image elements, and each element $o(x_n, y_m)$ is a scalar representing the optical absorption of the absorber at the position of (x_n, y_m). The vector $\mathbf{y}_l$ denotes the received A-line at scanning position T_l, having K samples. The full data set **Y** for one complete linear scan consists of L discrete time A-lines.

Using surperposition and Eq. (2), $\mathbf{y}_l$ can be expressed as a sum of photoacoustic waves from all absorbers in the ROI **O**:

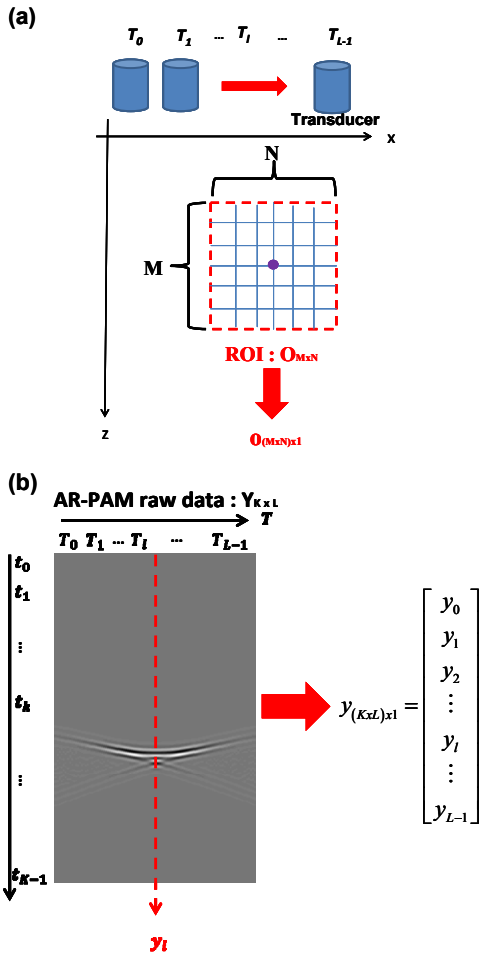

Figure 1. Illustration of sampling (a) AR-PAM data acquisition (b) AR-PAM raw data set

$$\begin{aligned} y_l &= \sum_{n=0}^{N-1}\sum_{m=0}^{M-1}\mathbf{h}_{\mathbf{SIR}}(T_l,x_n,y_m)\otimes\mathbf{h}_e\otimes\mathbf{p}\cdot o(x_n,y_m) \\ &= \sum_{n=0}^{N-1}\sum_{m=0}^{M-1}\mathbf{s}_l(x_n,y_m)\cdot o(x_n,y_m) \end{aligned}, \tag{3}$$

where $\mathbf{h}_{\mathrm{SIR}}(T_l, x_n, y_m)$ is the SIR vector from the transducer position T_l to $o(x_n, y_m)$, $\mathbf{h}_e$ and p are vectors of the electrical impulse response of the transducer and the photoacoustic waveform. After stacking the **Y** and **O** into column vectors: **y** and **o**, the model of the AR-PAM system can be expressed in the following matrix notiona [11][12]:

$$\mathbf{y} = \mathbf{So} + \mathbf{e}, \tag{4}$$

where **e** is a vector denoting additive noise, and **S** denotes

$$\mathbf{S} = \begin{bmatrix} S_0(0) & S_0(1) & \dots & S_0(N-1) \\ S_1(0) & S_1(1) & \dots & S_1(N-1) \\ \dots & & & \\ S_{L-1}(0) & S_{L-1}(1) & \dots & S_{L-1}(N-1) \end{bmatrix}$$

$$S_l(n) = (s_l(x_n, y_0) \dots s_l(x_n, y_{M-1})) \quad .$$

C. *Spatiotemporal optimal filter: deconvoling the SIR*

Based on Eq. (4), we can define a spatiotemporal optimal filter **K**, which minimize the synthetic aperture focusing error between **o** and **Ky** in the mean square error sense. Assume that both **o** and **e** are Gaussian, mutually uncorrelated random vectors with covariance matrices **Co** and **Ce**, respectively, the spatiotemporal optimal filter **K** can be found [11]:

$$\mathbf{K} = \mathbf{C_o}\mathbf{S}^{\mathrm{T}}(\mathbf{S}\mathbf{C_o}\mathbf{S}^{\mathrm{T}} + \mathbf{C_e})^{-1} \; . \qquad (5)$$

In this study, the filter **K** is responsible for synthetic aperture focusing.

III. SIMULATION RESULTS

In this section, simulations were performed to evaluate the efficacy of the proposed ISAFT for AR-PAM. All the simulations were done using the DREAM (Discrete Representation Array Modeling) Matlab toolbox [14]. The comparison between the proposed ISAFT and VD-SAFT were also carried out. Note that the results from our ISAFT were done without compensation for the electrical impulse response of the transducer in order to facilitate the comparison with the VD-SAFT algorithm that does not compensate the electrical impulse response of the transducer. The simulated transducer had a center frequency of 25 MHz, a diameter of 6 mm and a focal length of 12 mm (i.e., f-number = 2). The grid size of the region of interest was 0.02 mm, and the signal sampling rate was 500 MH. Point absorbers in front of and beyond the focal point were simulated to verify the efficacy on the improvement of synthetic aperture focusing.

Figures 2 and 3 show the original, VD-SAFT, and ISAFT images of the simulated point absorbers located in front of and beyond the focal point, respectively. The point absorbers are located at the depth of 10 mm, 11 mm, 13 mm, and 14 mm. All the AR-PAM images are envelope-detected images, and are displayed on a 30-dB dynamic range. It is evident that the proposed ISAFT offers better improvement in not only spatial resolution but also sidelobe suppression than VD-SAFT over all the simulated imaging depths because the full geometry of the VD, instead of the simplified virtual-point-detector approximation, is taken into consideration. In addition, more uniform image quality is also provided by the proposed ISAFT.

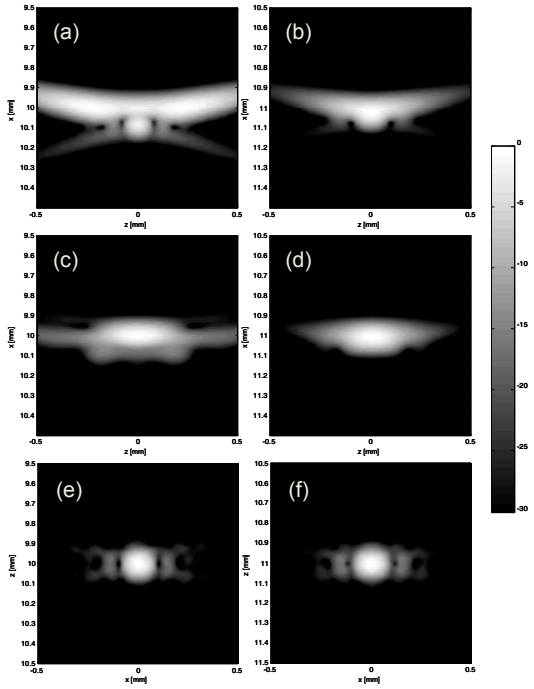

Figure 2. Envelope-detected AR-PAM images for a simulated point absorber in front of the focal point of the transducer. (a), (c), and (e): the point absorber is located at the depth of 10 mm; (b), (d), and (f): the point absorber is located at the depth of 11 mm. (a), (b): original; (c), (d): VD-SAFT; (e) and (f): ISAFT. Images are displayed on a 30-dB dynamic range.

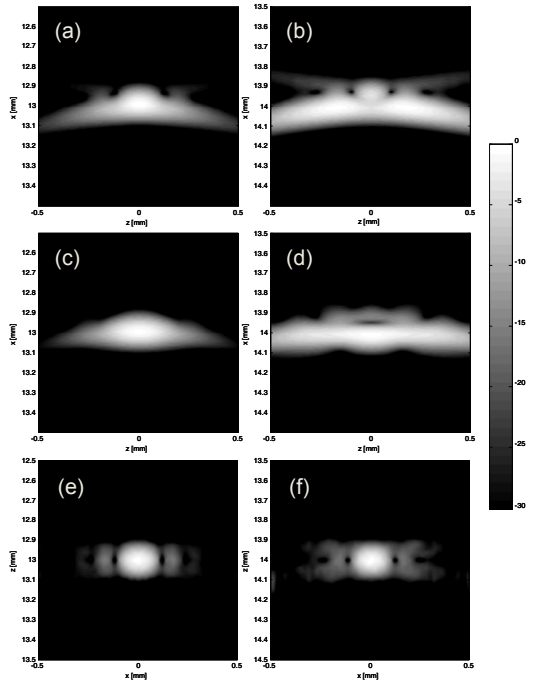

Figure 3. Envelope-detected AR-PAM images for a simulated point absorber beyond the focal point of the transducer. (a), (c), and (e): the point absorber is located at the depth of 13 mm; (b), (d), and (f): the point absorber is located at the depth of 14 mm. (a), (b): original; (c), (d): VD-SAFT; (e) and (f): ISAFT. Images are displayed on a 30-dB dynamic range.

IV. CONCLUSIONS

It is demonstrated by simulation that the proposed method effectively improves the degraded lateral resolution in the out-of-focused region for AR-PAM. The improvement in spatial resolution and sidelobe suppression of ISAFT is superior to that of VD-SAFT because the full geometry of the VD, instead of the simplified virtual-point-detector approximation, is taken into consideration. Future work will focus on the phantom and in vivo experimental verifications and the study of the effect of signal-to-noise ratio on the ISAFT.

ACKNOWLEGMENTS

Supports from National Science Council, Taiwan (NSC 97-2221-E-007-084-MY3) are greatly appreciated.

REFERENCES

[1] L. V. Wang, "Tutorial on photoacoustic microscopy and computed tomography," *IEEE J. Sel. Top. Quantum Electron.*, vol. 14, pp. 171-179, 2008.

[2] G. F. Lungu, M.-L. Li, X. Xie, L. V. Wang, and G. Stoica, "In vivo imaging and characterization of hypoxia-induced neovascularization and tumor invasion," *International Journal of Oncology*, vol. 30, pp. 45, 2007.

[3] M.-L. Li, J. C. Wang, J. A. Schwartz, K. L. Gill-Sharp, G. Stoica, and L. V. Wang, "In vivo photoacoustic microscopy of nanoshell extravasation from solid tumor vasculature," *J. Biomed. Opt.*, vol. 14, pp. 010507, 2009.

[4] P. H. Wang, J.-J. Luh, W.-S. Chen, and M.-L. Li, "*In vivo* photoacoustic micro-imaging of microvascular changes for Achilles tendon injury on a mouse model," *Biomed. Opt. Express*, vol. 2, pp. 1462-1469, 2011.

[5] M.-L. Li, J.-T. Oh, X. Y. Xie, G. Ku, W. Wang, C. Li, G. Lungu, G. Stoica, and L. V. Wang, "Simultaneous molecular and hypoxia imaging of brain tumors in vivo using spectroscopic photoacoustic tomography," Proc. IEEE, vol. 96, pp. 481-489, 2008.

[6] J. T. Oh, M.-L. Li, H. F. Zhang, K. Maslov, G. Stoica, and L. V. Wang, "Three-dimensional imaging of melanoma skin cancer in-vivo by dual wavelength photoacoustic microscopy," *Journal of Biomedical Optics*, vol. 11, pp. 034032-1, 2006.

[7] K. Maslov, G. Stoica, and L. V. Wang, "In vivo dark-field reflection-mode photoacoustic microscopy," *Optics Letters*, vol. 30, pp. 625–627 2005.

[8] L.-D. Liao, M.-L. Li, H.-Y. Lai, Y.-Y. I. Shih, Y.-C. Lo, S. Tsang, P. C.-P. Chao, C.-T. Lin, F.-S. Jaw, and Y.-Y. Chen, "Imaging brain hemodynamic changes during rat forepaw electrical stimulation using functional photoacoustic microscopy," *NeuroImage*, vol. 52, pp. 562-570, 2010.

[9] M. L. Li, W. J. Guan, and P. C. Li, "Improved synthetic aperture focusing technique with applications in high-frequency ultrasound imaging," *IEEE Trans. Ultrason., Ferroelec., Freq. Contr.*, vol. 51, pp. 63–70, 2004.

[10] M. L. Li, H. F. Zhang, K. Maslov, G. Stoica, and L. V. Wang, "Improved in vivo photoacoustic microscopy based on a virtual-detector concept," *Opt. Lett.*, vol. 31, pp. 474–476, 2006.

[11] M.-L. Li, Y.-C. Tseng, and C.-C. Cheng, "Model-based correction of finite aperture effect in photoacoustic tomography," *Opt. Express*, vol 18, pp. 26285-26292, 2010.

[12] F. Lingvall, T. Olofsson, and T. Stepinski "Synthetic aperture imaging using sources with finite aperture: Deconvolution of the spatial impulse response," *J. Acous. Soc. Am.*, vol. 114, pp. 225-234, 2003.

[13] B. Piwakowski and K. Sbai, "A new approach to calculate the field radiated from arbitarily structured transducer arrays," *IEEE Trans. Ultrason. Ferroelec., Freq. Contr.*, vol. 46, pp. 422-440, 1999.

[14] F. Lingvall, "Time domain reconstruction methods for ultrasonic array imaging," Ph.D. dissertation, Signals and Systems, Uppsala University, Uppsala, Sweden, 2004.